AMMONIA DISSOCIATION FOR SOLAR THERMOCHEMICAL ABSORBERS

BY

O M WILLIAMS AND P O CARDEN

DEPARTMENT OF ENGINEERING PHYSICS

RESEARCH SCHOOL OF PHYSICAL SCIENCES

THE AUSTRALIAN NATIONAL UNIVERSITY

CANBERRA, A.C.T., AUSTRALIA.

SUBMITTED TO THE INTERNATIONAL JOURNAL

OF ENERGY RESEARCH

JULY 1978

AMMONIA DISSOCIATION FOR SOLAR THERMOCHEMICAL ABSORBERS

by

O M Williams and P O Carden

Department of Engineering Physics
Research School of Physical Sciences
The Australian National University
Canberra, A.C.T., AUSTRALIA.

ABSTRACT

A prototype ammonia dissociator has been constructed and operated over a wide variety of conditions and its performance has been examined in relation to solar thermochemical absorber operation. High values of energy storage efficiency approaching unity are obtained for high values of reaction extent, corresponding to the use of high activity ammonia dissociation catalysts. There is a need for further development of such catalysts designed specifically for solar absorber operating conditions. It is shown that in order to make optimum use of the available catalyst volume, the power density profile and specific absorber design should be matched to give an essentially isothermal temperature profile along the catalyst chamber length. There is potential for a solar thermochemical absorber based on ammonia dissociation to be constructed using simple tube technology and thus within the severe cost constraints associated with solar absorber design.

1. INTRODUCTION

Thermochemical energy transfer systems show considerable promise for transferring energy from a distributed solar collector array to a central plant. A number of reversible reactions have been proposed [1-5] as suitable for thermochemical energy transfer but to date there has been little experimental work supporting the proposals. In two previous papers [6,7], we have developed the fundamental thermodynamic theory underlying the operation of such systems and in this paper we describe experiments designed to test the high pressure ammonia dissociation reaction

$$NH_3 \rightleftharpoons \frac{3}{2}H_2 + \frac{1}{2}N_2$$

proposed by Carden [1] as the basis of solar thermochemical absorber operation. A prototype ammonia dissociator has been designed and operated over a wide variety of conditions and its performance has been correlated with that expected on the basis of known heat exchanger and catalyst chamber operation. Experiments performed with the dissociator have identified several characteristic features of thermochemical energy transfer processes and these are discussed in detail with particular reference to solar thermochemical absorber operation. It is found that in order to make optimum use of the available catalyst volume, the power density profile and the specific design of the absorber should be matched to give an essentially isothermal temperature distribution along the catalyst chamber length. High values of thermochemical energy storage efficiencies approaching unity are obtained for high values of reaction extent,

corresponding within the cost constraints associated with solar absorber design to the use of a high activity ammonia dissociation catalyst. There is a need for further development of such a catalyst, designed specifically for withstanding the thermal cycling and high pressure, high temperature conditions inherent in solar thermochemical absorber operation.

2. DISSOCIATOR CONSTRUCTION

Development of a large scale solar power plant is associated with severe cost constraints, particularly in relation to the energy collection and energy transport systems. Carden [1] has shown that in order to compete economically with an oil-fired thermal power plant with oil costed at 10 $/barrel, the combined installed costs of the energy collection and energy transport systems in a solar power plant can amount to no more than $50 per square metre of collector area, or no more than $50 per peak kilowatt of incident solar radiation (1976 US dollars). The cost of the solar absorber would not be expected to account for more than 10-15% of this allowance and therefore a successful design must be conceptually simple. Although the present dissociator has been designed primarily for testing the feasibility of thermochemical energy transfer systems, the experiments have been conducted with the additional motivation of showing that a solar thermochemical absorber based on the ammonia dissociation reaction has potential for meeting the cost constraints.

The present dissociator has been designed following preliminary measurements from earlier prototypes and is shown in Figure 1. The dissociator consists essentially of a tubular

counterflow heat exchanger welded to a cylindrical multichannel catalyst chamber, the latter being heated electrically. The heat exchanger consists of a thin wall 1.5 mm diameter hypodermic tube (304 stainless steel) inside the bore of a 16 SWG 1/4 inch tube (316 SS). Nickel spirals have been wound both inside and outside tha bore of the hypodermic tube in order to promote turbulent fluid flow and hence efficient heat transfer across the tube wall. The outside tube is lagged with calcium silicate thermal insulation.

Ammonia liquid is pumped through the inner tube where it comes into thermal contact with the hot reaction mixture flowing in the opposite direction within the space between the inner and outer tubes. The ammonia is thus preheated and conversely, the hot reaction mixture is cooled towards ambient temperatures. At the hot end of the heat exchanger, the ammonia passes to the catalyst chamber. The chamber has been constructed by drilling 54 parallel 3.1 mm diameter holes longitudinally around the circumference and through the 90 mm length of a 3 inch bore schedule 40 incoloy 800 tube. Incoloy 800 has high strength and high resistance to nitriding in an ammonia atmosphere at high temperatures. The parallel holes form catalyst channels and are connected by 1.5 mm diameter holes cut at an angle of 30° to the tube axis through the common wall of neighbouring channels. Each channel is packed with 2.2 mm x 2.2 mm x 4.0 mm pellets of ICI 47-1 ammonia dissociation catalyst and is sealed at each end (except for the input and output ports) by incoloy 800 plugs which have been interference fitted and welded to the main body.

Interchannel connections have been cut so that the input ammonia passes along the length of the first channel and then divides into two streams which pass in opposite directions up and down successive channels around the tube wall towards the output channel. The ammonia dissociates as it passes along the two counterflowing multichannel paths. The two streams are recombined at the final channel of the catalyst chamber and the reaction mixture then passes to the hot end of the heat exchanger and thence along the heat exchanger length to the connecting pipework.

The reactor is heated electrically and uniformly by a coil of stainless steel sheathed Pyrotenex heating wire wound around the circumference of the incoloy tube. The tube and heater combination is lagged by 6 cm thickness of calcium silicate insulation. Catalyst chamber temperatures are measured by sheathed iron-constantan thermocouples inserted into the gas stream through selected end plugs. The heat exchanger thermocouples are spot-welded to the outer heat exchanger jacket. Input power levels to the dissociator are measured by precision voltmeter and ammeter.

The dimensions of the catalyst channels have been chosen so that the dissociator is capable of withstanding simultaneous high temperature and high pressure operation for a useful experimental life. Strength calculations based on 12000 psi design stress at 700°C and 5000 psi operating pressure indicate a rupture life of 5000 hours and 2% creep after 1000 hours of operation. These limits are quite adequate for an experimental device but would need to be upgraded for a working solar thermochemical absorber.

3. DISSOCIATOR EXPERIMENTS

Commercial grade anhydrous ammonia is compressed and pumped into the bottom of a high pressure hydraulic accumulator prefilled with nitrogen at typically 150-200 atmospheres. At the same time ammonia is pumped into the bottom of a gravitational separation chamber. The nitrogen is compressed as the volume of ammonia increases and pumping is continued until the accumulator and separator are both half-filled. The accumulator and separator are then isolated from the compressor and ammonia is circulated through a flow control valve to the dissociator. Volume flow rates are measured to within 1% accuracy by a miniature turbine flowmeter developed in this laboratory (Whelan [8]) and are converted to mass flow rates through use of known ammonia densities. System pressures are measured by Bourdon gauges.

The reaction mixture from the dissociation chamber separates spontaneously into gas and liquid phases as the ammonia condenses within the heat exchanger and is passed to the gravitational separator. Liquid ammonia is drawn from the bottom of the separator and is pumped back to the accumulator. The gas production is drawn through an output throttle valve which is set to maintain constant system pressure and passes at ambient pressure through a condenser operated at -60°C where residual ammonia vapour is removed. The flow rate of the gas stream is then measured by a Gilmont rotameter and is corrected to account for gas volume changes within the high pressure system arising from the finite ammonia consumption.

3.1 Thermal Analysis

Dissociation experiments at pressures in the range 50-200 atmospheres were conducted over a range of input power levels up to 2.5 kW and a range of ammonia flow rates. A typical temperature profile is shown in Figure 2. Heat leaks through the thermal insulation were identified by similar experiments using high pressure nitrogen in place of ammonia. Detailed energy balance of the temperature profiles recorded for nitrogen using known specific heats identified the localities and magnitudes of heat leaks common to the ammonia dissociation and nitrogen experiments. Secondary corrections were applied to the magnitudes of the heat leaks in order to account for the differences between the two temperature profiles, thus allowing the nett power input after subtracting the losses to be determined at each point along the dissociator length. For an experiment in which 1.5 kW is absorbed from the heater under conditions of 0.5 g/s ammonia flow rate and 40% dissociation by weight, the energy distribution is typically

Absorbed chemical energy	950 W
Thermal energy in outlet fluid	250 W
Heat leak through catalyst chamber insulation	150 W
Heat leak through heat exchanger insulation	50 W
Heat leak through thermocouple ports	100 W

Considerable improvement in conduction losses would be effected for a working thermochemical solar absorber optimized for minimum cost.

4. ANALYSIS

4.1 Ammonia/Hydrogen-Nitrogen Thermodynamics

The fundamental thermodynamic processes underlying the operation of thermochemical energy transfer systems have been studied in two recent papers [6,7] from this laboratory and, in particular, the thermodynamic efficiencies for the ammonia/hydrogen-nitrogen system have been calculated. It has been necessary as part of the calculational procedure to generate thermodynamic data not available within the chemical engineering literature. The data is available in detailed form elsewhere (Williams [9,10]).

The principal thermodynamic features of the ammonia/hydrogen-nitrogen system are reproduced for convenience in the temperature-enthalpy diagram shown in Figure 3. The ammonia characteristic curve for each pressure exhibits strong curvature in the region where the latent heat of vaporization (or effective latent heat) is absorbed, whereas the hydrogen-nitrogen curve is characterised by essentially constant specific heat. The curves for intermediate mixtures follow the hydrogen-nitrogen curve within the single phase region above the dew line but on the other hand, show pronounced curvature within the two-phase region where ammonia liquid condenses from the fluid mixture. The lines for chemical equilibrium drawn in Figure 3 define the maximum extent to which the reaction can proceed at each value of temperature and pressure.

4.2 Counterflow Heat Exchanger Operation

For energy balance at all points z along the length of the counterflow heat exchanger the thermal equilibrium conditions

$$\dot{m}c_{p1}\frac{dT_1}{dz} = U_L(T_2 - T_1) \tag{1}$$

and

$$\dot{m}c_{p2}\frac{dT_2}{dz} = U_L(T_2 - T_1) + 2\pi K_{cs}\frac{T_2 - T_s}{\ln\left(1 + \frac{t_{cs}}{r_{cs}}\right)} \tag{2}$$

where the subscripts 1 and 2 refer to the feed and return channels respectively, must be satisfied. U_L represents the composite heat transfer coefficient per unit length and is related to the individual coefficients according to

$$\frac{1}{U_L} = \frac{1}{h_{L1}} + \frac{1}{h_{L2}} + \frac{\ln\left(1 + \frac{t_m}{r_m}\right)}{2\pi K_m} \tag{3}$$

(see, for example, Zemansky [11]). The latter terms in (2) and (3) represent the influence of conduction through the calcium silicate insulation and across the heat exchanger membrane respectively. Values for the film coefficients h_L in circular pipes are related [11] to the fluid conditions according to

$$h_L \propto c_p Pr^{-0.6}\mu^{0.2}\left(\frac{\dot{m}}{d}\right)^{0.8} \tag{4}$$

where d is the pipe inner diameter and $\dot{m}$ is the mass flow rate. The pressure and temperature variations of the Prandtl number Pr and viscosity μ for the ammonia/hydrogen-nitrogen system are calculated elsewhere [10].

The heat exchanger temperature profile may be explained readily by reference to the system thermodynamics shown in Figure 3 and to the energy balance equations (1) and (2) (neglecting to first order the conduction loss term in (2)). The counterflow heat exchanger operates with ammonia flowing in the feed channel and the reaction mixture from the catalyst chamber flowing in the return channel. It is clear from Figure 3 that the specific heat of any two-phase mixture exceeds that of ammonia for temperatures below that of the dew temperature of the mixture. Conversely, above the dew temperature, the specific heat of ammonia exceeds that of the return mixture. Towards the cold end of the exchanger, therefore, the temperature of the ammonia feed must according to (1) and (2) rise more steeply with distance than the temperature of the return fluid in order to retain local energy balance. For a heat exchanger of sufficient length, this rise continues until the two temperatures are almost equal at the dew temperature, as seen in Figure 2. Moreover, since the thermal capacity of the return fluid exceeds that of the ammonia feed throughout the low temperature region, the ammonia feed cannot accept all the available heat from the return fluid. The return fluid temperature does not therefore fall to the ammonia feed temperature at the heat exchanger outlet and finite heat is neccessarily carried from the exchanger in the form of sensible heat. In a distributed collector solar power plant, this heat would not be used and would instead be wasted to the surroundings. Thus the sensible heat carried from the exchanger represents a real inefficiency, the magnitude of which is discussed below in Section 5.1.

Above the dew temperature the specific heat of the ammonia feed exceeds that of the return fluid, as seen from Figure 3. The curvature of the temperature profile is therefore reversed with the return fluid now having insufficient heat capacity to supply the heat requirements of the input ammonia stream. The temperature of the ammonia feed does not therefore reach the return fluid temperature at the hot end of the heat exchanger, as seen in Figure 2.

4.2 Catalyst Chamber Operation

Heat is applied uniformly throughout the length of the catalyst chamber with minor deviations from uniformity caused by finite conduction around the cylindrical wall. Circumferential conduction occurs as a direct result of the non-uniform temperature distribution around the tube wall and its effect has been included in the present analysis.

Specific heats within the catalyst chamber operating range are essentially constant (see Figure 3) so that in the absence of heat leaks and finite dissociation it would be expected that the temperature would rise linearly along the catalyst chamber length. When dissociation occurs, heat is drawn from the supply to provide the endothermic heat of reaction, leaving insufficient heat available to maintain a linear rise. The temperature profile across the catalyst chamber therefore assumes a characteristic curved profile as seen in Figure 2.

The variation of reaction extent with distance may be deduced from the observed temperature profile and from the differential power input $d\dot{Q}/dz$ obtained from the known power input after allowing for circumferential conduction and for thermal losses through the insulation. The relation

$$\frac{d\dot{Q}}{dz} = \dot{m}[(1 - \delta)c_p + \delta c'_p]\frac{dT}{dz} + \frac{\dot{m}\Delta H}{M}\frac{d\delta}{dz} \qquad (5)$$

must be satisfied for local energy balance, allowing the weight fraction $\delta(z)$ of product gas mixture to be determined by successive integration along the catalyst chamber length, starting from $\delta = 0$ at the reactor inlet. The form of $\delta(z)$ as derived from (5) is shown in Figure 2.

The spatial variation of $\delta(z)$ is related to the ammonia dissociation reaction rate which is given most commonly by the Temkin-Pyzhev relation (Vancini[12])

$$\frac{df_{NH_3}}{dt} = -k(T)\left[\left(\frac{f^2_{NH_3}}{f^3_{H_2}}\right)^{1-\alpha} - K_f f_{N_2}\left(\frac{f^3_{H_2}}{f^2_{NH_3}}\right)^{\alpha}\right] \qquad (6)$$

in terms of the partial fugacities f of the components and the equilibrium constant K_f for the reaction

$$2NH_3 \rightleftharpoons 3H_2 + N_2$$

The exponent α assumes a value close to 0.5 for most catalysts. Equation (16) is not strongly pressure dependent (varying as $p^{-0.5}$ far from equilibrium) but is strongly temperature dependent through the Arrhenius relationship for catalyst activity

$$k(T) = k_o \exp\left(-\frac{E_A}{kT}\right) \tag{7}$$

where the intrinsic activity k_o is proportional to the catalyst volume and where E_A is the activation energy. By the equation of continuity, the reaction rate given by (6) must also satisfy the relation

$$\frac{\dot{m}}{A}\frac{d\left(f_{NH_3}/\rho(z)\right)}{dz} = \frac{df_{NH_3}}{dt} \tag{8}$$

where A is the catalyst tube area and where $\rho(z)$ is the fluid density. Within the dissociation region above 750°K, both ammonia and the hydrogen-nitrogen mixture may be treated to first order as approximate ideal fluids, in which case f_{NH_3} may be approximated by the partial pressure

$$P_{NH_3} = \frac{1 - \delta}{1 + \delta} P \tag{9}$$

and the fluid density by

$$\rho(z) = \frac{MP}{RT(1 + \delta)} \tag{10}$$

where M is the molecular weight of ammonia and P is the system pressure. Substitution of (9) and (10) into (8) leads to the result that

$$(1 - \delta)\frac{dT}{dz} - T\frac{d\delta}{dz} = \frac{AM}{R\dot{m}}\frac{df_{NH_3}}{dt} \tag{11}$$

Given the observed spatial variation of temperature and the spatial variation of δ calculated from (5), as illustrated in Figure 2, the catalyst activity k(T) may be computed from (6) and

(11) over the complete range of dissociation temperatures. The temperature dependence for k(T) as derived from a number of separate experiments is shown in the Arrhenius plot, Figure 4. All experiments were performed after the catalyst had been fully reduced.

It is clear from Figure 4 that the ammonia dissociation experiments are described well by the Temkin-Pyzhev rate equation, the standard Arrhenius form for temperature dependence being followed even at low values of fractional dissociation where the rate equation (6) must eventually fail. The activation energy obtained for the nickel catalyst from the slope of Figure 4 is 84 Kcal/mole which is rather larger than the value of 38 Kcal/mole typical of promoted iron synthesis catalysts (ICI Catalyst Handbook [13]). This result suggests that considerable improvement could be achieved by development of more active catalysts designed specifically for high pressure ammonia dissociation under the conditions likely to be encountered by solar thermochemical absorbers.

4.4 Dissociator Simulation

Given that values for the heat transfer coefficient U_L and the catalyst activity k(T) have been deduced from the ammonia dissociation experiments described above, it is possible to reverse the analysis and simulate the dissociator operation for a given ammonia flow rate and given power input by numerical integration of the two pairs of coupled differential equations (1) and (2), and (5) and (11). Constant reaction rates are assumed

for $\delta < 0.03$ since in this range reaction rates tending towards infinity are predicted by the Temkin-Pyzhev equation (6) as δ tends towards zero. The full curves in Figure 2 have been obtained by computer simulation of the dissociator operation with the constant of proportionality in (4) used as a fitting parameter in the heat exchanger region, and the full curve in Figure 4 used to describe catalyst activity. The heat exchanger fitting constant corresponds to values of U_L of typically 0.24 W cm^{-1} K^{-1} for an ammonia flow rate of 1 g/s.

Excellent agreement has been obtained between the observed and calculated temperature profiles shown in Figure 2 thus allowing the computer simulation to be used with some confidence for a detailed parametric examination of the dissociator operation. The results of this examination are described below.

5. DISCUSSION

It is evident from the preceding description that a substantial fraction of the input power to a high pressure ammonia dissociator can be transformed into chemical form provided that care is taken to minimize conduction losses. The fundamental processes occurring in the dissociator have been identified successfully and in the following sections are used to explain the characteristic features of solar thermochemical absorber operation. Losses due to heat leaks which may be reduced by increasing insulation thickness and quality are not considered here. The magnitude of such losses is dependent on the absorber size and specific design and will be studied in later work.

5.1 Heat Exchanger Thermal Loss

We have shown above in Section 4.2 that a finite amount of energy is carried from the dissociator in the form of residual sensible heat in the output fluid mixture. Such low grade heat could not be tapped successfully in a solar power plant based on a distributed array of solar collectors and therefore a real loss is introduced into the system. The origins of the heat loss are shown elsewhere [6,7] to be related to the thermodynamic requirement that the work required to separate ammonia liquid from the output fluid mixture must be developed internally within the system. The magnitude of the loss is determined in terms of the energy storage efficiency η_{ST} which is defined in [6] as

$$\eta_{ST} = \frac{\text{Chemical energy transferred to storage}}{\text{Nett thermal energy absorbed from source}}$$

Values of η_{ST} calculated in [7] for the ammonia/hydrogen-nitrogen system are reproduced in Figure 5. It is seen that, apart from in the region of low δ, η_{ST} increases steadily with increasing δ and approaches unity as the dissociation reaction approaches completion. Energy storage efficiency may therefore be maximised by ensuring that a solar thermochemical absorber operates such that the dissociation reaction proceeds as far as practical towards completion. The magnitude of the loss is related closely to the heat exchanger outlet temperature and in our previous study [7] we have shown good agreement between the thermodynamic predictions of outlet temperature and the measurements from the present dissociator.

5.2 The Dissociation Catalyst

The relationship between the maximum dissociator temperature and input power level for the present dissociator (catalyst volume = 30 cm^3) is shown in Figure 6. Evidently, high power levels of the order of 3 kWt can be attained but only at temperatures of the order of 800°C at the catatyst chamber outlet. At such temperatures, the strength of incoloy 800 falls rapidly with increasing temperature and it would be preferable if the dissociator were operated at a lower temperature of typically 700-720°. Satisfactory operation at lower temperatures would require either a larger catalyst volume or use of a more active catalyst.

The ICI 47-1 nickel catalyst used in the present experiments has not been designed for operation in high pressure thermochemical energy transfer systems. The catalyst is in fact used commercially at ambient pressure for complete dissociation of ammonia to provide a convenient source of industrial hydrogen, and as such is therefore unlikely to be the ideal choice for the present requirements. Curves of constant reaction rate calculated from (6) and (7) appropriate to the measured activation energy of 84 Kcal/mole are shown in Figure 7. Since materials are likely to limit the maximum operating temperature, it is clear from Figure 7 that the maximum reaction extent for a given reaction rate curve is also limited and therefore greater levels of dissociation can only be obtained for a given catalyst if the reaction rate is increased. This corrresponds either to greater catalyst volume or to increased intrinsic activity. Alternatively, higher reaction

rates at the required temperatures may be obtained by using a catalyst characterised by higher activation energy, such as one of the promoted iron catalysts used in ammonia synthesis. Since it is important to achieve high reaction rates and hence high reaction extents in order to attain high efficiency operation, as shown in Figure 6, there is a need to study such catalysts from the point of view of examining their capability of withstanding the high temperature operation and the thermal cycling inherent in solar thermochemical absorber operation.

5.3 Solar Thermochemical Absorber Operation

This far, we have considered that heat is applied uniformly along the length of the catalyst volume as in the present experiments. However, as shown for example in Figure 8, the power density profile estimated for one possible system design, the cavity absorber-paraboloidal concentrator combination, is far from uniform, high power levels occurring at the mouth of the cavity and decreasing levels occurring as the distance from the cavity mouth increases. Similar non-uniform profiles are likely to be encountered for most absorber-collector combinations since large amounts of energy are collected at large angles from the outer areas of the paraboloid compared to the energy collected at small angles.

In the case of the cavity absorber-paraboloidal concentrator combination, particular advantage may be taken of the non-uniform energy density profile when the catalyst chamber is constructed in the form of a single cylindrical coil filled with catalyst, rather

than in the multichannel longitudinal design of the present dissociator. When the coil is wound within the cavity as shown in Figure 8 such that the preheated ammonia is passed from the heat exchanger to the cavity mouth, then the higher power levels encountered there would lead to a steeper temperature gradient along the the initial part of the catalyst bed. Higher reaction rates are therefore attained within a shorter distance and greater use is made of the available catalyst volume. Ideally, the cylindrical windings would be spaced within the cavity so that an isothermal temperature distribution occurred along the catalyst bed. The same design criterion would need to be applied to alternative absorber designs such as the hemispherical assembly proposed by Carden [1].

Although the present treatment is rather simplistic (with unity absorbtance assumed for the catalyst tube wall and no account taken of heat transfer limitations through the wall to the catalyst), a reasonable guide to the temperature and reaction extent profiles corresponding to the power density profile of Figure 8 may be gained by computer simulation, as shown in Figure 9. It is seen that an approximately isothermal temperature profile has been obtained over much of the catalyst chamber length and comparison with Figure 2 shows that for the same overall power input the maximum operating temperature has fallen from 750°c to 725°C. This fall represents an increase in rupture life by a factor of 3.5 and therefore a significant decrease in the anticipated installed cost of the dissociator. It is clear that considerable advantage may be gained if the power density profile and catalyst chamber design are matched so that the dissociator

operates isothermally. Further study of solar absorber aperation is required for a detailed assessment of performance including the limitations of specific designs, heat transfer rates and heat losses.

5.4 Absorber Thermal Response

In this section attention is drawn to one final feature of interest which is evident from the operational characteristics shown in Figure 7; namely, the thermal response of an ammonia dissociator to changes in input power level. Such changes will occur regularly in a solar power plant as clouds obscure the sun. For the present dissociator operated with an ammonia flow rate of 1 g/s, a fall in input power from 3 kWt to 1 kWt leads to a fall in maximum temperature from 820°C to 665°C, with the energy storage efficiency falling from 95% to 70%. Thus, the power input at lower insolation levels is still absorbed effectively even though the fluid flow rate is unchanged. Under similar conditions, the same power change for a water/superheated steam system operated normally at 550°C would cause the operating temperature to fall to 250°C. Such a fall could not be tolerated at the input of a steam turbine and it would therefore be necessary to provide individual flow regulators at each collector, servoed to the level of incident power. Regulators are not only potentially unreliable but also would increase significantly the capital cost of the energy transport system. In contrast, a thermochemical energy transfer system does not require temperature-controlled regulators since the reaction rate and

output temperature adjust automatically to match the input power level. Thermal time lags are also reduced since (provided heat leaks and radiation losses are small) the absorber will assume a high quiescent temperature for relatively long periods when clouds obscure the sun. These features relate directly to the rapid temperature change of catalyst activity and together represent a significant advantage for solar thermochemical absorbers over absorbers based on steam generation.

6. SUMMARY

In this paper we have described experiments designed to test the feasibility of using the ammonia dissociation reaction as the basis for a solar thermochemical energy transfer system. The conversion from thermal to chemical energy has been demonstrated for a prototype high pressure ammonia dissociator and operational knowledge has lead to a thorough understanding of the design requiements for practical solar thermochemical absorbers. It has been demonstrated that in order to make optimum use of the available catalyst volume, the power density profile to a solar thermochemical absorber should be tailored to give an essentially isothermal temperature profile along the catalyst chamber length. High energy storage efficiencies approaching unity are obtained for high values of reaction extent and these are obtained when catalysts of high activity are used for solar thermochemical absorber operation. There is a need for improvement in the ammonia dissociation catalysts available for this purpose.

The design of solar thermochemical absorbers is subject to severe cost constraints and it is therefore necessary that a suitable design be neither complicated nor large. It has been shown in this paper that an ammonia dissociator operated within an absorber cavity could be constructed in the form of a single coil of high pressure tubing filled with catalyst together with a tubular counterflow heat exchanger. The specific design details including the effects of scaling in absorber size compared to collector size need to be examined in more detail for this and alternative absorber assemblies. It is apparent, however, that the strengths of the design rest on the inherent simplicity of tube technology and lend some confidence that the cost constraints can be met, particularly if the absorber were operated with an improved high activity catalyst. Such a catalyst would be required to withstand the high temperature, high pressure operation and the conditions of irregular thermal cycling inherent in the operation of solar thermochemical absorbers.

ACKNOWLEDGEMENTS

The high pressure ammonia dissociator described in this paper was constructed by Mr D.C.Hall. Mr Hall also assisted at the design stage and his invaluable contribution is gratefully acknowledged. The project also benefitted from design and technical assistance by Messrs H.P.Cantor, K.Erick and R.E.Whelan and their services are also gratefully acknowledged.

REFERENCES

[1] P O Carden, Solar Energy 19, 365 (1977).

[2] T A Chubb, Solar Energy, 17, 129 (1975).

[3] A F Hildebrandt, Solar Tower Thermochemical Energy Cycles, Hydrogen Energy Fundamentals Symposium-Course, Miami, Florida (1975).

[4] W Hafele, Science, 84, 360 (1974).

[5] W E Wentworth and E Chen, Solar Energy, 18, 205, (1976).

[6] P O Carden and O M Williams, submitted to the Int J of Energy Research.

[7] O M Williams and P O Carden, submitted to the Int J of Energy Research.

[8] R E Whelan, in preparation, to be submitted to J Phys E.

[9] O M Williams, Thermodynamic Data for the Ammonia Synthesis and Dissociation Reactions, Energy Conversion Technical Report No 11, Department of Engineering Physics, The Australian National University, Canberra, ACT, Australia, (1976).

[10] O M Williams, Generation of Thermochemical Energy Transfer Data for the Ammonia/Hydrogen-Nitrogen System, Energy Conversion Technical Report No 16, Department of Engineering Physics, The Australian National University, Canberra, ACT, Australia (1978).

[11] M W Zemansky, Heat and Thermodynamics, McGraw Hill, New York, (1957).

[12] C A Vancini, Synthesis of Ammonia, Macmillan, London, (1971).

[13] Catalyst Handbook, ICI Ltd, Wolfe, London, (1970).

NOMENCLATURE

A	Catalyst tube cross-sectional area
c_p	Specific heat of ammonia
c'_p	Specific heat of hydrogen-nitrogen
c_{p1}, c_{p2}	Specific heat of heat exchanger input and output fluids
d	Heat exchanger inner diameter
E_A	Activation energy
f_i	Partial fugacity of component i
h_L	Convective heat transfer coefficient per unit length
ΔH	Reaction heat
$k(T)$	Rate constant for ammonia dissociation
k_o	Intrinsic activity
K_f	Equilibrium constant
K_{cs}	Thermal conductivity of insulation
K_m	Thermal conductivity of heat exchanger membrane
$\dot{m}$	Mass flow rate
M	Molecular weight of ammonia
P	System pressure
Pr	Prandtl number
$\dot{Q}$	Input power
r_{cs}	Insulation radius
r_m	Heat exchanger membrane radius
R	Gas constant
t	Time
t_{cs}	Insulation thickness
t_m	Heat exchanger membrane thickness
T	Absolute temperature
T_S	Ambient temperature

T_1, T_2	Heat exchanger input and output fluid temperatures
U_L	Overall heat transfer coefficient per unit length
z	Distance along heat exchanger or catalyst chamber
δ	Weight fraction of hydrogen-nitrogen in mixture
η_{ST}	Energy storage efficiency
μ	Viscosity
ρ	Fluid density

FIGURE CAPTIONS

Figure 1 Schematic diagram of the ammonia dissociator. The catalyst chamber consists of 54 parallel channels drilled longitudinally in the wall of a 9 cm length of incoloy 800 tube. Only the inlet and outlet channels are shown in the diagram.

Figure 2 Characteristic temperature profile and reaction extent profile of the ammonia dissociator operated under conditions of uniform power density applied along the catalyst chamber length. The full curves represent the best computer simulation of the experimental points. $\dot{m}$ = 0.46 g/s, P = 150 atmospheres. Absorbed power (excluding heat leaks) = 1000 W. Catalyst volume = 30 cm^3.

Figure 3 Temperature-enthalpy characteristics for the system ammonia/3:1 hydrogen-nitrogen.

Figure 4 Arrhenius plot of catalyst activity derived according to the Temkin-Pyzhev equation for ICI 47-1 ammonia dissociation catalyst. The full line represents the best fit through the experimental points. Activation energy = 84 Kcal/mole.

x 60 atm

o 100 atm

●, + 150 atm

Figure 5 Energy storage efficiencies for the system ammonia/3:1 hydrogen-nitrogen (T_S = 295°K).

Figure 6 Thermal capacity and efficiency for the ammonia dissociator of Figure 1 operating at 300 atmospheres with uniform power density. Catalyst volume = 30 cm^3.

_____ Maximum dissociator temperature

------ Energy storage efficiency.

Figure 7 Curves of constant reaction rate in decade steps for ammonia dissociation using ICI 47-1 catalyst. Activation Energy = 84 Kcal/mole.

Figure 8 (a) Schematic diagram of a cavity absorber associated with a 65° rim angle paraboloidal concentrator, showing the cylindrically wound tubular catalyst chamber suitable for isothermal ammonia dissociation.

(b) Differential power input to the cavity wall (assuming unity absorbtance on the catalyst tube wall).

Figure 9 Temperature profile and reaction extent profile appropriate to the differential power input shown in Figure 8(b).

$\dot{m}$ = 0.46 g/s , P = 150 atmospheres

Absorbed power = 1000 W

Catalyst volume = 30 cm^3.

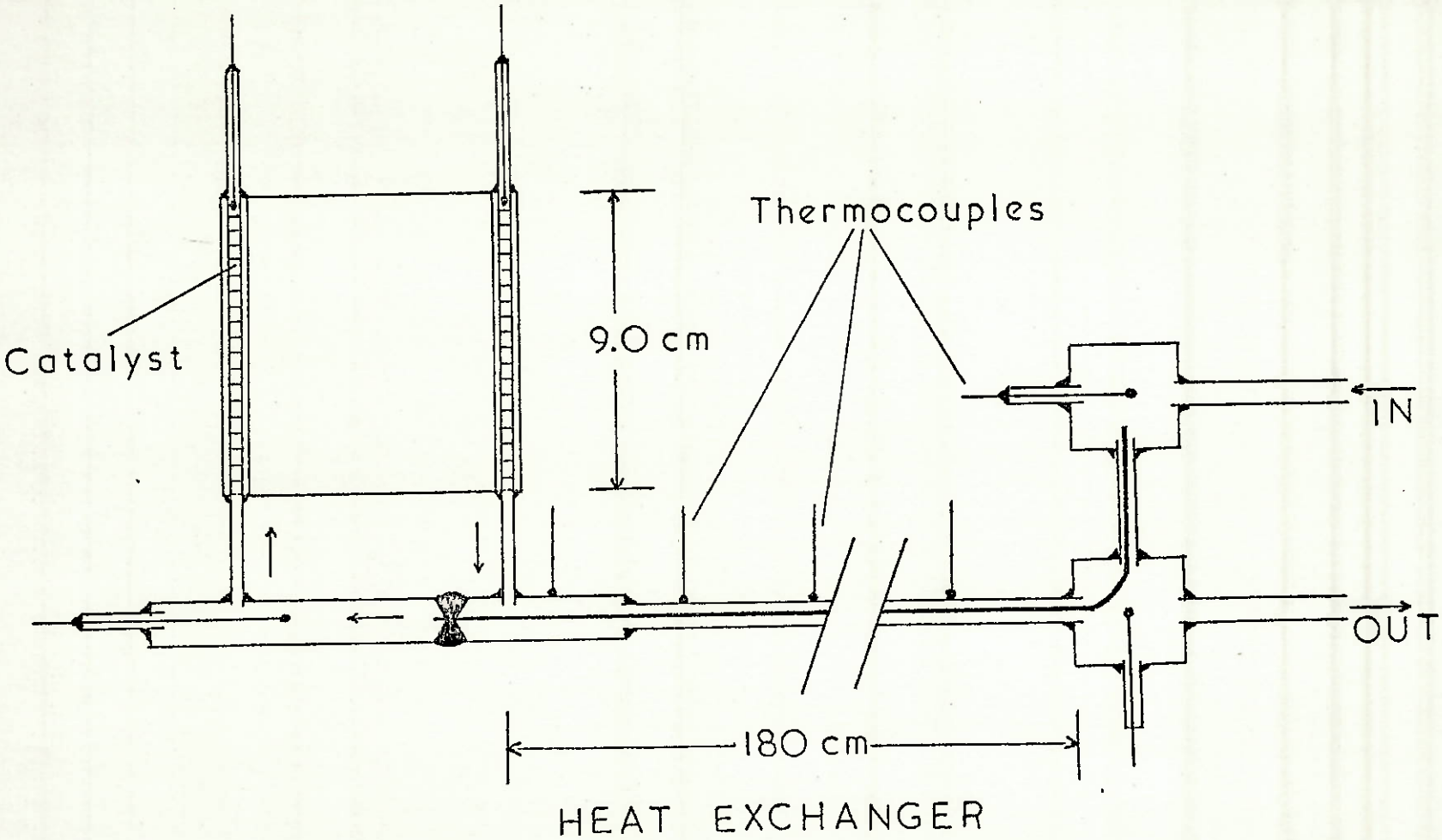

FIGURE 1: Schematic diagram of the ammonia dissociator. The catalyst chamber consists of 54 parallel channels drilled longitudinally in the wall of a 9 cm length of incoloy 800 tube. Only the inlet and outlet channels are shown in the diagram.

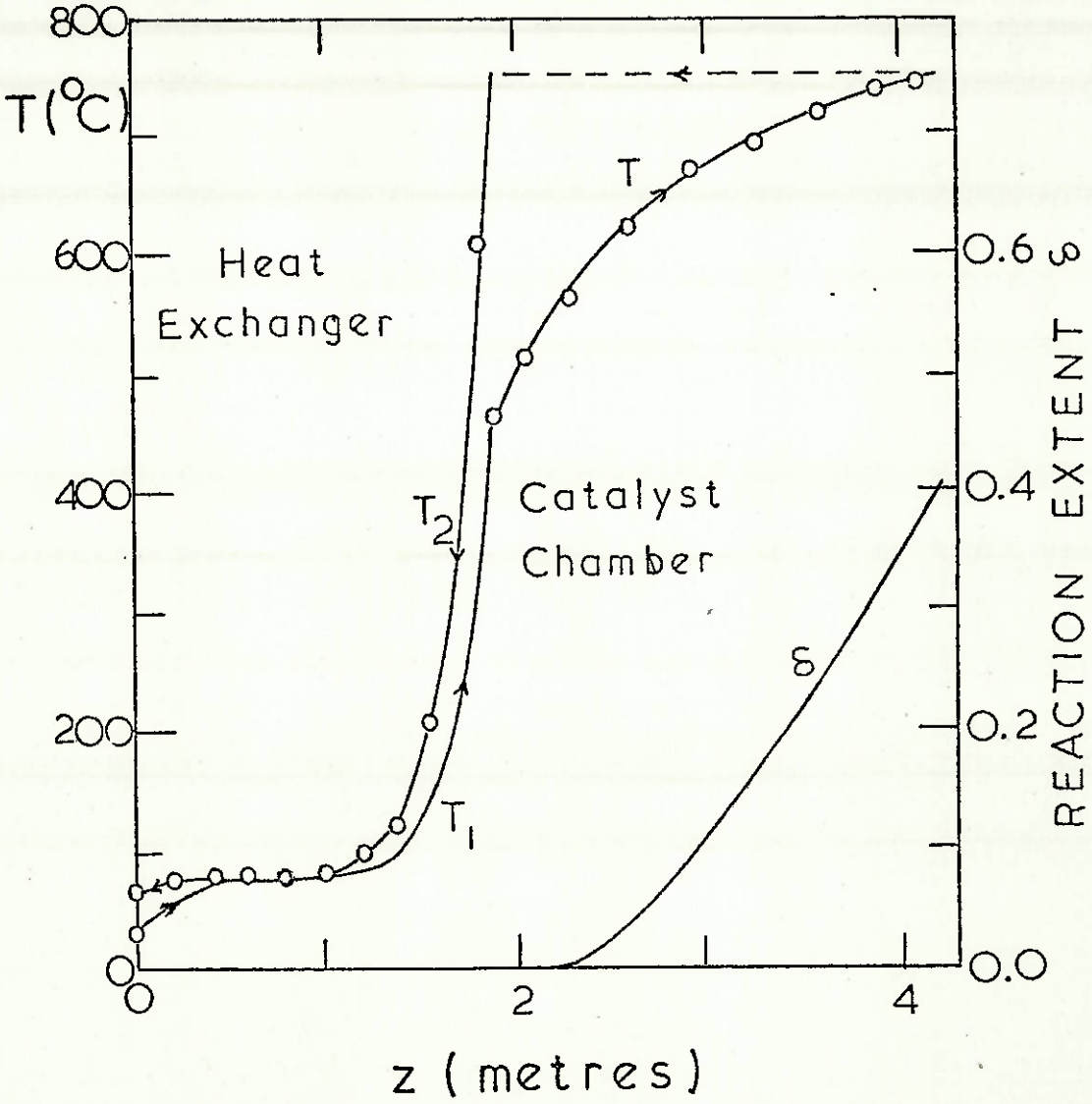

FIGURE 2: Characteristic temperature profile and reaction extent profile of the ammonia dissociator operated under conditions of uniform power density applied along the catalyst chamber length. The full curves represent the best computer simulation of the experimental points. $\dot{m}$ = 0.46 g/s, P = 150 atmospheres. Absorbed power (excluding heat leaks) = 1000 W. Catalyst volume = 30 cm^3.

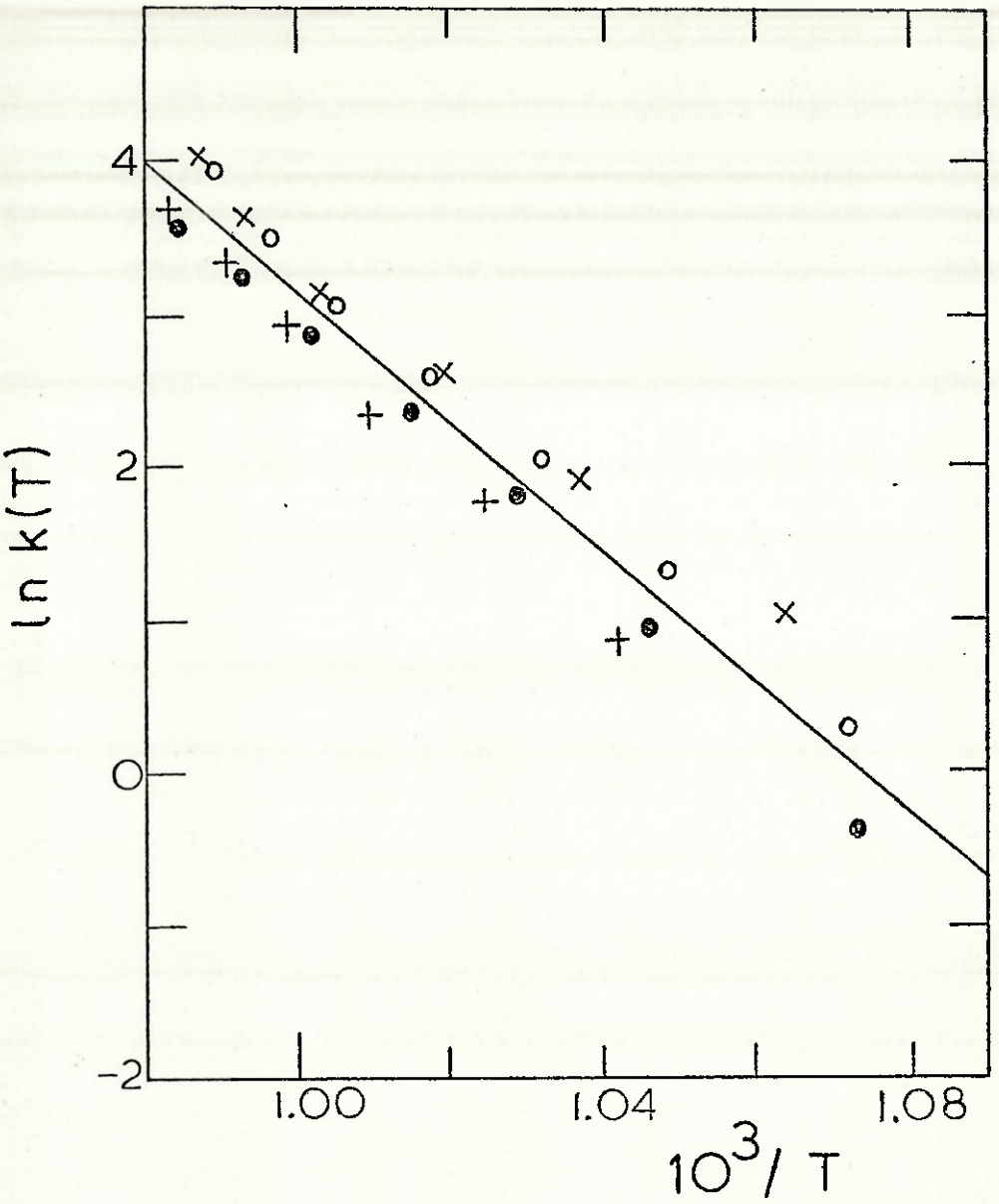

FIGURE 4: Arrhenius plot of catalyst activity derived according to the Temkin-Pyshev equation for ICI 47-1 ammonia dissociation catalyst. The full line represents the best fit through the experimental points. Activation energy = 84 Kcal/mole.

x 60 atm

o 100 atm

●, + 150 atm

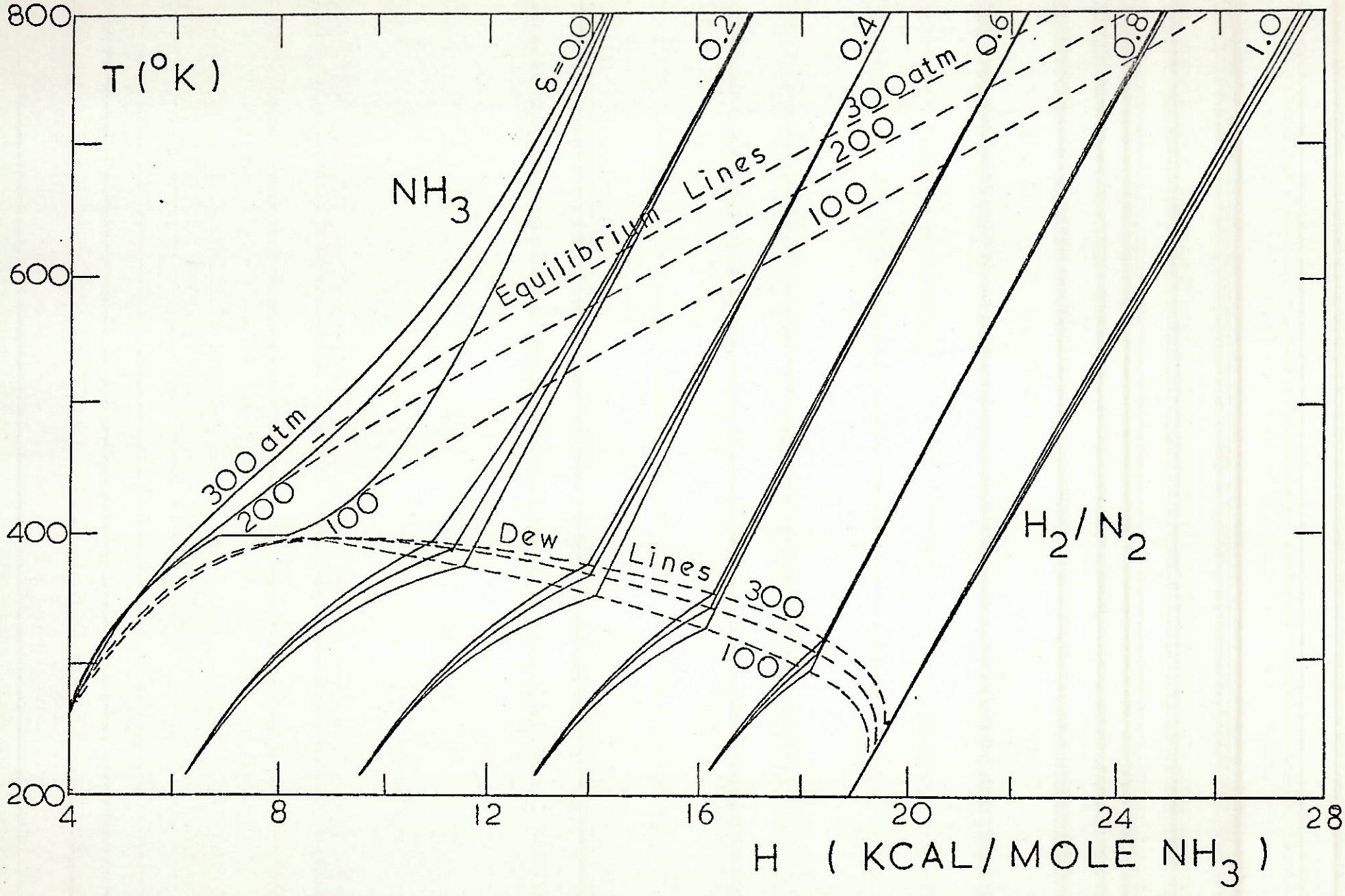

FIGURE 3: Temperature-enthalpy characteristics for the system ammonia/3:1 hydrogen-nitrogen.

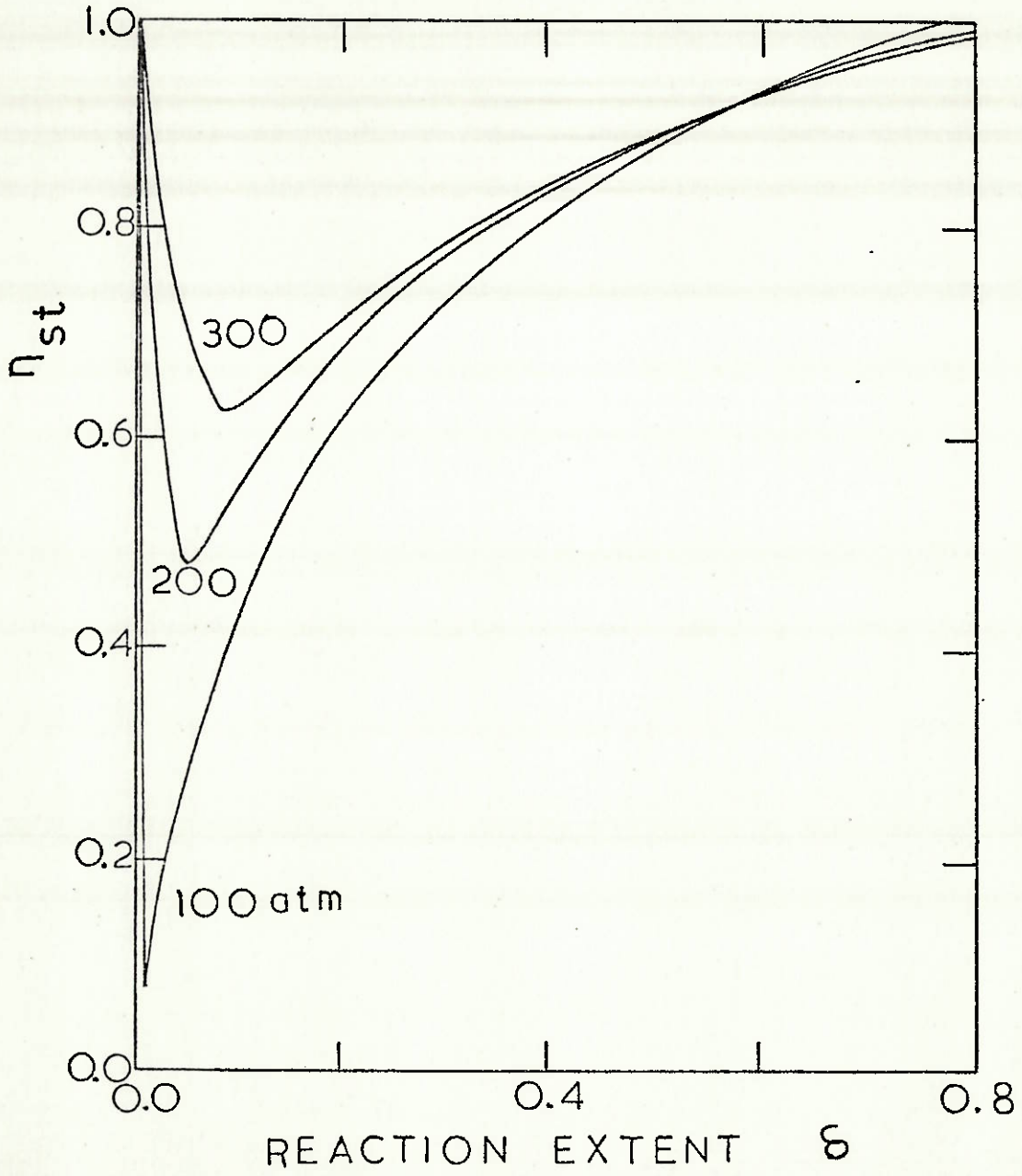

FIGURE 5: Energy storage efficiencies for the system ammonia/3:1 hydrogen-nitrogen (T_S = 295°K).

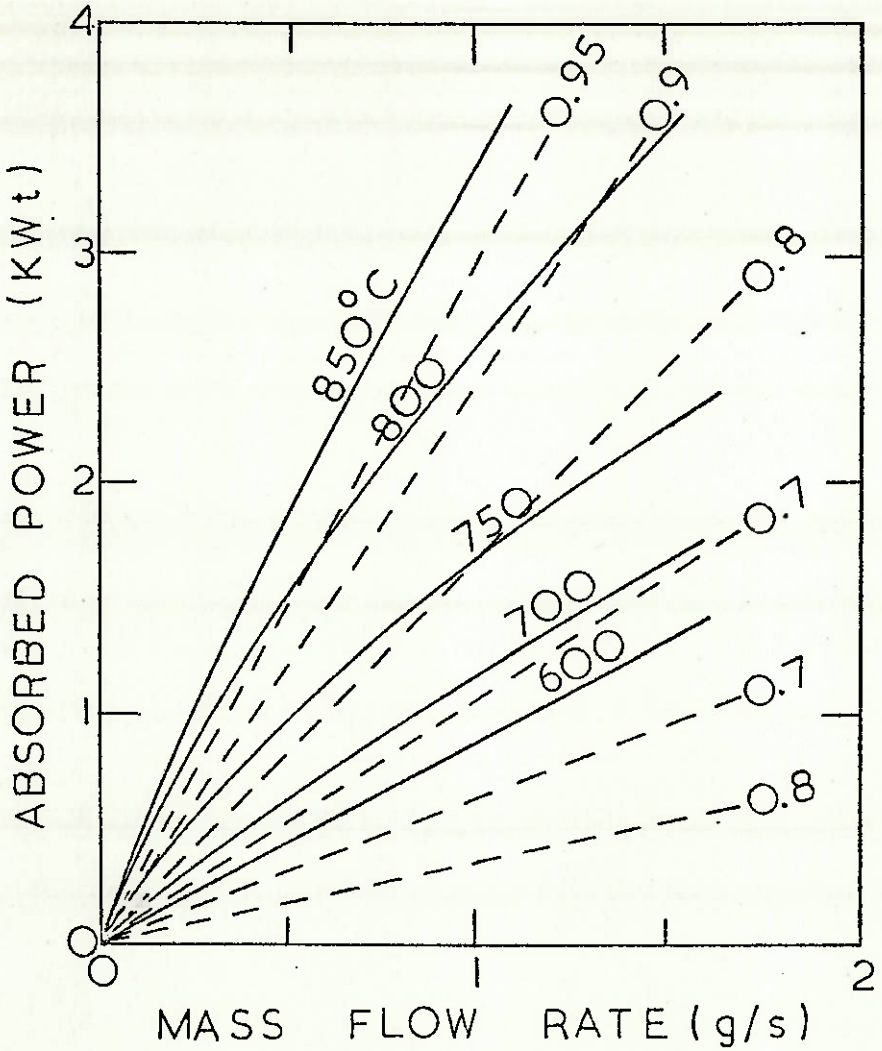

FIGURE 6: Thermal capacity and efficiency for the ammonia dissociator of Figure 1 operating at 300 atmospheres with uniform power density. Catalyst volume = 30 cm^3.

——— Maximum dissociator temperature

------ Energy storage efficiency

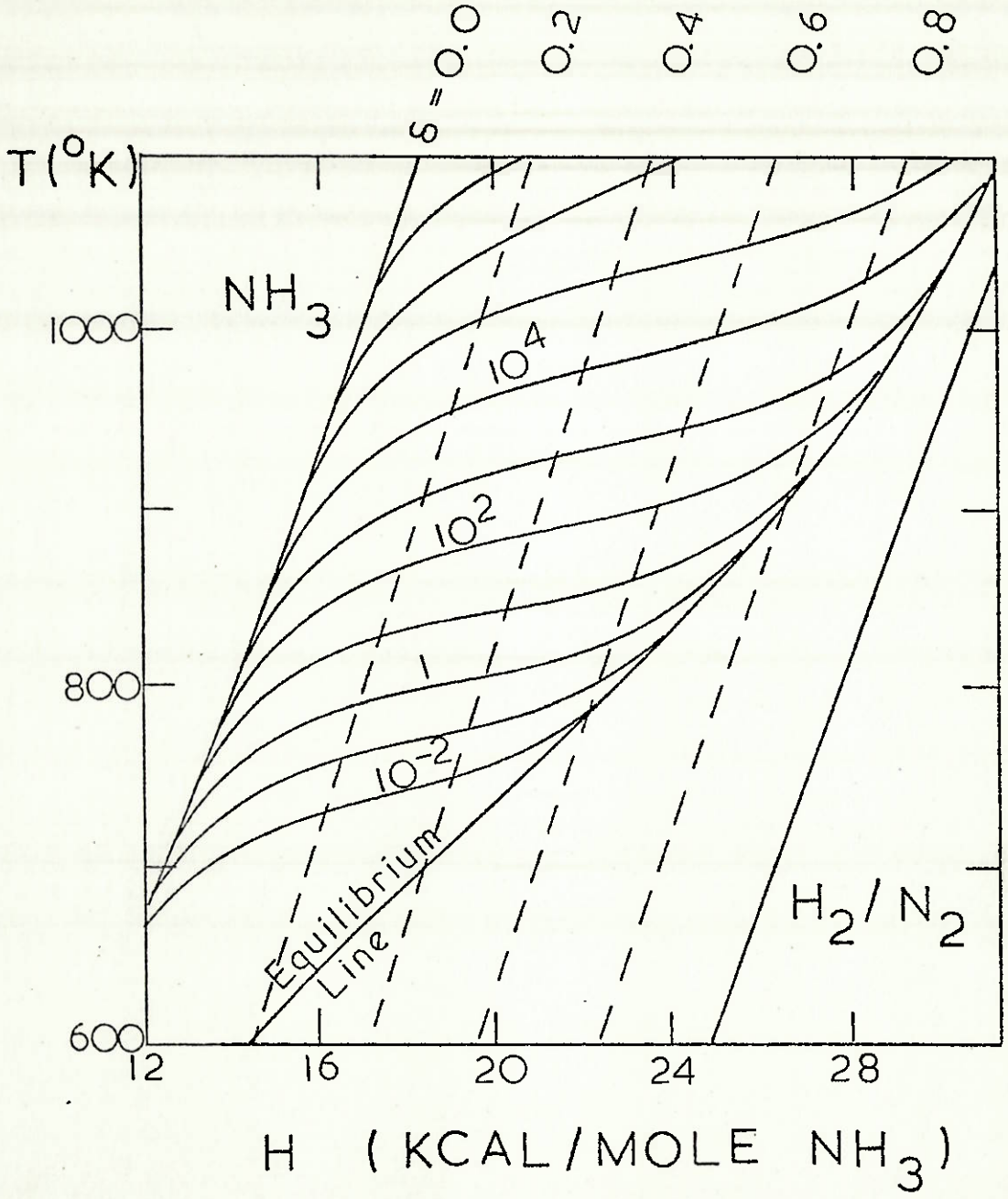

FIGURE 7: Curves of constant reaction rate in decade steps for ammonia dissociation using ICI 47-1 catalyst. Activation energy = 84 Kcal/mole.

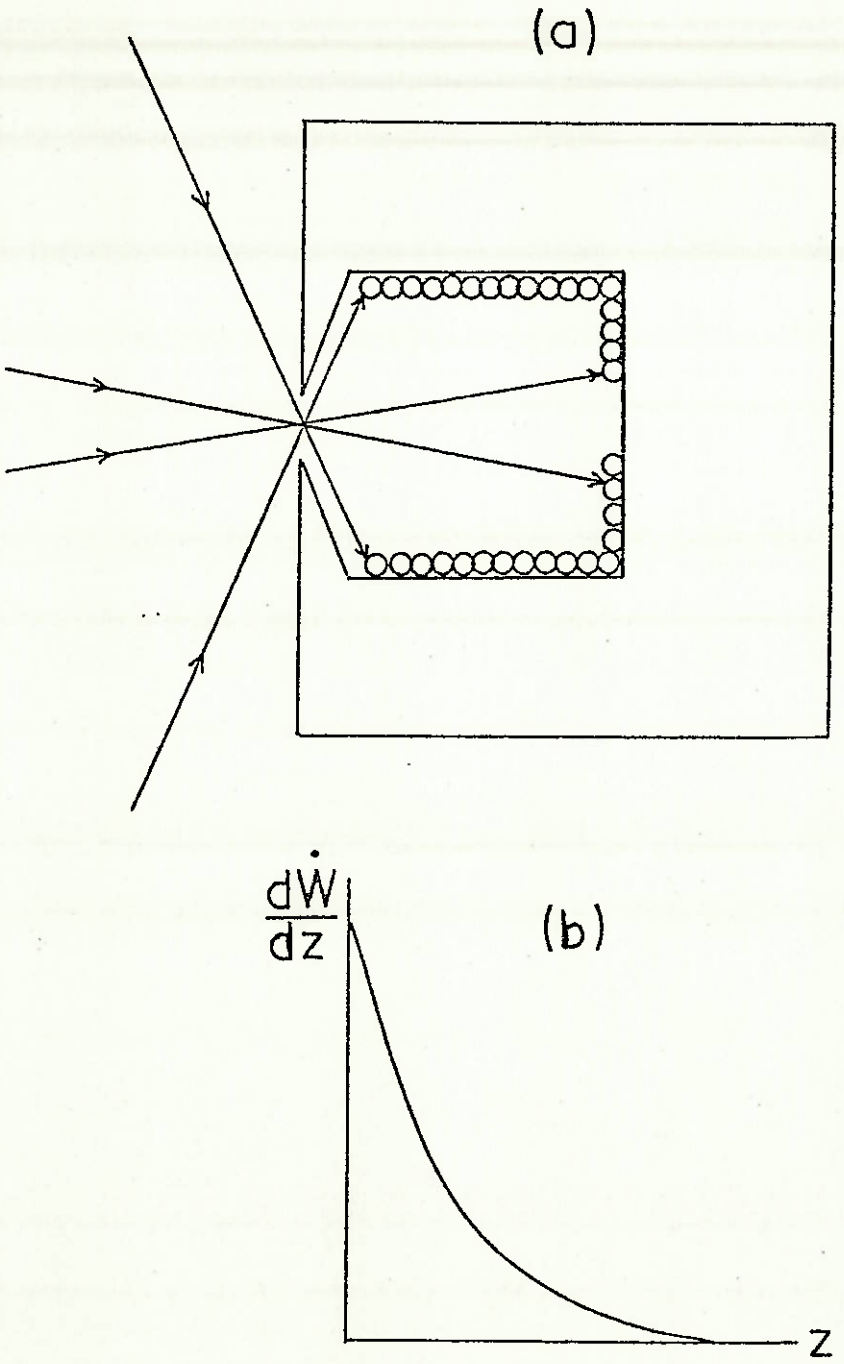

FIGURE 8: (a) Schematic diagram of a cavity absorber associated with a 65° rim angle paraboloidal concentrator, showing the cylindrically wound tubular catalyst chamber suitable for isothermal ammonia dissociation.

(b) Differential power input to the cavity wall (assuming unity absorbtance on the catalyst tube wall).

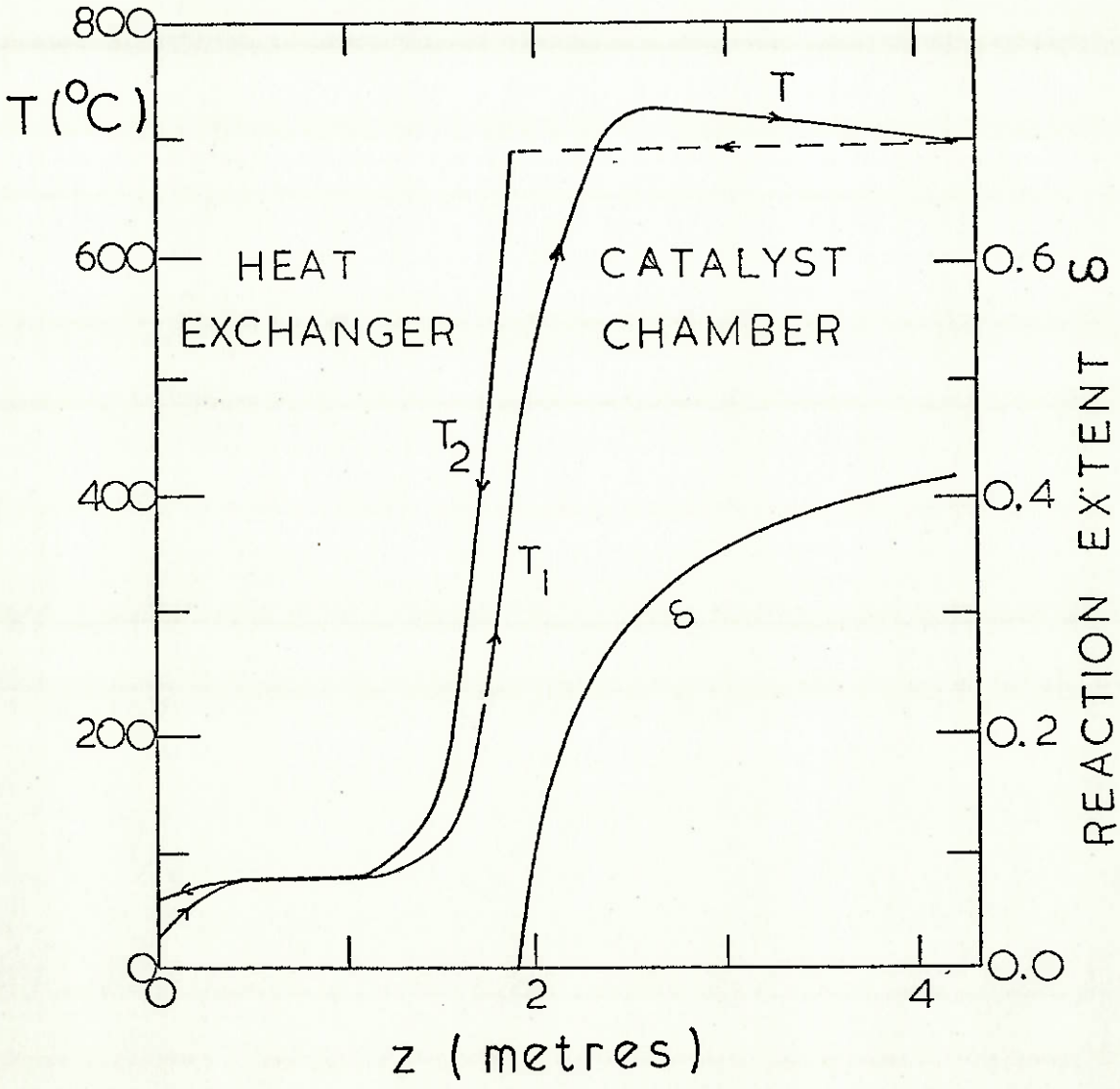

FIGURE 9: Temperature profile and reaction extent profile appropriate to the differential power input shown in Figure 8(b).
$\dot{m}$ = 0.46 g/s, P = 150 atmospheres
Absorbed power = 1000 W
Catalyst volume = 30 cm^3